Performance of the GSN station SSE-IC, 1996-2009

A report in a series documenting the status of the Global Seismographic Network

WQC Report 2010:10
March 4, 2010

Göran Ekström and Meredith Nettles

Waveform Quality Center
Lamont-Doherty Earth Observatory of Columbia University, New York

1 Station performance report: SSE

This report summarizes a number of observations that are relevant for assessing the past and current quality of the data recorded at one of the stations of the Global Seismographic Network. The purpose of the report is, in part, to document specific problems observed with the data. Some of these problems are related to errors in the available descriptions of station parameters: orientation of the sensors, response functions, polarities. In principle, such errors in the station metadata can be corrected by providing updated station parameters. In practice, this may be difficult in some cases due to lack of knowledge of, or inability to determine, the correct parameters. Other problems are caused by the malfunctioning of some instrument component. Regardless of the cause, it is necessary to document and publicize the lack of accurate and reliable station characteristics, especially when it is not obvious from simple inspection of the data that a problem exists. It is also of value to document the characteristics of stations performing well, both to establish their high quality and to help identify installation and operation procedures that should be emulated at other stations.

1.1 Station SSE

The station SSE (Shanghai) is located in the suburbs of the city of Shanghai in eastern China (see Figure 1). It is in a very good location for providing global coverage in earthquake, nuclear monitoring, and Earth structure studies. The closest GSN station is TATO-IU (Taipei) in Taiwan, approximately 700 km south of SSE.

SSE is part of the New China Digital Seismograph Network (network code IC) and is maintained by the USGS.

1.2 The data

Digital broadband seismic data from SSE-IC are available from the IRIS DMC beginning in 1996. Prior to becoming a station of the New China Digital Seismograph Network, SSE was a station of the China Digital Seismograph Network (CDSN, network code CD) (1986–1996). Here, we consider very-broad-band GSN instruments at the station beginning in 1996. The GSN installation in 1996 consisted of a set of STS-1 seismometers. An auxiliary STS-2 sensor was installed in 1999. Data from SSE are included in our standard CMT analysis (Dziewonski et al., 1981; Ekström et al., 2005), and waveform data, travel-time

observations, and dispersion curves derived from SSE data have been used in the development of numerous global and regional tomographic models since the station was installed.

In the analyses described here, we have made use of data collected from the IRIS DMC. We requested and downloaded all long-period (LH) and very-long-period (VH) data available at the DMC for both sensors from the start of operation (1996) until September 2009. We used the currently available station metadata prepared by the Albuquerque Seismological Laboratory and available at the IRIS DMC (downloaded in December 2009). Overall, the station has been operated with few data outages since 1996.

1.3 The metadata

The dataless SEED volume for SSE documents 2 response epochs for the STS-1 (primary) and STS-2 (secondary) sensors at SSE. The STS-1 1 sps channels were initially called LHZ, LHN, LHE, without a location code. They were renamed with the location code 00 on 1999.189 (189 representing the day of year). We refer to these channels as LHZ-00, LHN-00, and LHE-00. The STS-2 sensor (location code 10) was installed on 1999.189 and we refer to the 1 sps channels as LHZ-10, LHN-10, and LHE-10. Epoch boundaries are given at 1996.263 (first data) and 1999.189 (first STS-2 data). The metadata indicate no changes in the STS-1 responses at the epoch boundaries.

1.4 Scaling analysis

One method for assessing the quality of the data is the systematic comparison of recorded long-period waveforms with synthetic seismograms calculated for known seismic events. This analysis follows the steps described by Ekström et al. (2006). Seismic data for the LH and VH channels from both the STS-1 and STS-2 sensors are collected. Corresponding synthetic waveforms for all earthquakes in the Global CMT catalog (Dziewonski et al., 1981; Ekström et al., 2005) with $M_W \geq 6.5$ are calculated. Correlation coefficients and optimal scaling factors between observed and synthetic waveforms are calculated for the three types of data used in the standard CMT analysis: body waves (B), with periods in the range 50–150 sec, mantle waves (M), with periods in the range 125–350 sec, and surface waves (S), with periods in the range 50–150 sec. Body- and mantle-wave results are discussed here. The scaling factor is only calculated for waveforms with a correlation of 0.75 or greater. The scaling factor is the number by which the synthetic seismogram should be multiplied to maximize the agreement with the observed seismogram. Annual median values of the scaling factors are calculated when four or more individual event scaling estimates are available for the year. Reversed components can be identified by their large negative correlations.

Figure 2 shows the results of our systematic comparison of SSE waveforms with synthetic seismograms. The diagram illustrates several problems with the data. Good correlation of all three components of the primary sensor with synthetic waveforms is only seen during 1996–2000. Starting in 2000, the N–S component mantle waves are too small with respect to the synthetic waveforms. By 2004, the scaling factor is less than 0.5. The scaling factors for STS-1 and STS-2 seismograms are significantly different from each other for all three components, suggesting a problem with absolute (frequency-independent) calibration.

An abrupt change in the scaling factor for the vertical-component STS-2 seismograms is seen in 2006, suggestive of a sudden loss of gain. Throughout the period of operation, very few horizontal-component mantle-wave seismograms recorded on the STS-2 sensor are of sufficient quality to correlate well with the synthetic waveforms.

1.5 Noise analysis

A second method for investigating the overall performance of the sensors is to monitor background noise levels for all seismic channels, after conversion of the data to ground acceleration. We calculate hourly rms

values of the time-domain seismic signal in narrow frequency bands, and convert the rms values to a power spectral density (PSD) at that frequency using Parseval's theorem. For each month, we then calculate the low-noise value at each frequency by determining the PSD amplitude not exceeded 10% of the time.

The PSD data provide much information about the station and the sensors. Figure 3 shows the monthly low-noise estimate for each LH channel at 72-s period since 1996. The first observation is that the station has been providing data without major outages since 1996. Second, the noise data indicate that SSE was a very quiet site for all STS-1 components in 1996–2000. Noise levels on the vertical and N–S STS-1 increased by more than 10 db in 2001, returning to lower levels by 2002. Both components show increasing noise since 2002, with the N–S noise level increasing more rapidly. Noise levels on the E–W component have been high, and highly variable, since 2001.

STS-2 vertical noise levels were low immediately following installation in 1999, increased 5–10 db in 2000, and dropped in 2006 (probably associated with an instrument problem, as seen in Figure 2). Noise levels on the horizontal components of the STS-2 are very high, and have recently been variable.

1.6 Inter-sensor coherence

An additional method for assessing the quality and calibration of the recorded signals is to calculate inter-sensor coherence. This analysis is possible when more than one sensor is operated in the same location. At SSE, this is possible for the period 1999–2009, during which time both STS-1 and STS-2 instruments have operated.

We calculate the coherence of the deconvolved vertical, N–S, and E–W components. The coherence is calculated for ∼2-hour-long time windows containing the signals for earthquakes with $M_W \geq 6.5$ (the same events used in the scaling analysis). For each pair of seismograms, the coherence is calculated in narrow frequency bands around 32 s, 64 s, 128 s and 256 s. If the coherence is greater than 0.95, the value is stored together with the complex scaling factor (represented here as a scaling factor and phase shift) that should be applied to the secondary-sensor data to bring the two time series into the best agreement. In the following, the discussion is generally based on the assumption that the secondary (STS-2) sensor is properly calibrated and that deviations from a scaling factor of 1.0 and a phase shift of 0° should be attributed to differences between the true and reported response functions of the primary (STS-1) sensor. As noted earlier, there are clear problems with the STS-2 vertical component after 2006.

Figure 4 shows the results of the coherence analysis for the vertical component. The measurements are consistent and stable from 1999 until the beginning of 2006. For 1999–2006, there is a nearly frequency-independent deviation in the responses indicating a 15% too-high gain specified for the STS-1 sensor. In 2006, a sudden jump occurs in the scaling factor, consistent with a loss of gain of the STS-2 sensor by approximately one half. Simultaneously, frequency-dependent variations become more prominent, and a lack of long-period observations suggests a deterioration of the quality of the signal on one or both sensors.

Figure 5 shows the coherence results for the N–S component. The data are characterized by a frequency-independent deviation of ∼15%, present for the entire period of observation, and a loss of long-period gain of the STS-1 sensor starting in 2000, becoming most extreme in 2005–2008, and recovering slightly after 2008. The complete lack of measurements at 256 s is most likely due to the high noise level on the STS-2 sensor.

Figure 6 shows the results for the E–W component. This component shows primarily a frequency-independent deviation of ∼15%, and a lack of long-period (128-s and 256-s) observations, probably due to high noise levels on one or both sensors.

The gain offset of 10–20% for all three STS-1 components at SSE, and the loss of long-period gain for the N–S component, were described by Ekström et al. (2006). The loss of long-period gain is similar

to problems observed at other stations, such as KIP (Ekström and Nettles, WQC Report 2010:2) and DAV (Ekström and Nettles, WQC Report 2010:7).

1.7 Polarization analysis

The orientation of the horizontal components can be assessed empirically by comparing observed and synthetic waveforms, and finding the angle by which the horizontal components should be rotated in order to maximize the agreement. We follow the approach described by Ekström and Busby (2008) for such a comparison, using the observed and synthetic waveforms from Global CMT analysis.

We apply the method of Ekström and Busby (2008) to the same dataset used in the scaling analysis. Figure 7 shows the individual measurements for the period of operation for the different channels. The median rotation angles for the STS-1 are 7° for the LHN, LHE epoch of measurements, and 5° for the LHN-00, LHE-00 epoch. For the STS-2 the median angle is 5°. The spreads in the measurements are relatively small for both sensors. The larger scatter seen in the STS-1 (00) measurements after 2002 is likely a consequence of the malfunctioning N–S component.

The median estimates for the entire period of operation are given in Table 1. Experience gained in the study of Ekström and Busby (2008) suggests that both sensors are likely to be misoriented by $\sim 5^\circ$.

Comp. 1	Comp. 2	First	Last	# Obs.	N	Az 1	Az 2	25%	Med.	75%
LHE	LHN	19961009	19990615	95	28	90	0	3	7	10
LHE-00	LHN-00	19990711	20090930	402	123	90	0	1	5	11
LHE-10	LHN-10	19990711	20090930	402	131	90	0	2	5	10

Table 1: Statistics of sensor-rotation angles estimated in this study. Columns are the channel names, the dates of the first and last observations considered in making the estimate, the total number of observations, the number of observations of acceptable quality, the reported azimuths of sensitivity of the two channels, the median polarization-angle deviation from the reported orientation together with the range of the second (25%) and third (75%) quartiles of the observations.

1.8 Example seismograms

The anomalies described here agree with observations we have made in our routine analysis of waveforms for the determination of CMT earthquake parameters. When confronted with the seismograms for an individual earthquake, it is often difficult to assess whether a poor fit is due to incorrect source parameters, inadequate modeling of wave propagation through an Earth model, or some problem with the recorded seismograms. Here, we have included some examples of data that illustrate the characteristics of the types of problems that we have encountered with data from the SSE station.

Figure 8 shows an example of three-component mantle-wave data for an earthquake on December 2, 1996. This corresponds to a period during which the STS-1 sensor appears to have operated properly, and noise levels on all components are low. The correlation of observed and synthetic waveforms is high, greater than 0.93 for all components. The scaling factors for the three components (0.770, 0.728, 0.887) are consistent with the average (Figure 2) and suggest a problem with the overall gain of the STS-1 sensor.

The top panel of Figure 9 shows a comparison between mantle-wave seismograms recorded on the STS-1 seismometer (top panel) and the corresponding synthetic waveforms for an event on October 8, 2005. The N–S component is noticeably too small with respect to the synthetic seismograms, resulting in a scaling factor of 0.415. The seismograms from the STS-2 (bottom panel) are much noisier, but are well fit by the

synthetic waveforms. The scaling factor for the N–S seismogram is 1.257. The factor-of-three difference in the gain between the STS-1 and STS-2 N–S components is consistent with the results of the coherence analysis (Figure 5).

Figure 10 shows a comparison of body-wave seismograms from the STS-2 sensor and corresponding synthetic waveforms for an $M_W = 7.0$ earthquake on September 2, 2009. The small scaling factor for the STS-2 vertical seismogram (0.582) reflects the loss of gain on this component. The horizontal components of the STS-2 exhibit very high noise levels.

2 Summary and analysis

At the time of writing (March, 2010), the GSN station SSE is not performing well. The absolute (frequency-independent) calibration of the STS-1 sensor appears to be in error by $\sim$15%, as indicated by scaling analysis (Figure 2) and coherence analysis (Figures 4–6). The STS-1 N–S component displays a time-variable long-period loss of gain, and appears to have been malfunctioning since 2000.

The STS-2 sensor is very noisy on the horizontal components, and the vertical component lost half of its gain in early 2006, a change that is not reflected in the metadata. Data quality on the vertical component also appears to have deteriorated since 2006.

Polarization analysis indicates that both sensors are misoriented by $\sim 5^\circ$.

3 Conclusions and recommendations

Our analysis shows that SSE generated data of GSN quality only during the period 1996–2000. However, even during this time, the STS-1 gains appear to have been improperly specified. The station has suffered from a chronic STS-1 problem since 2000. The horizontal components of the STS-2 are remarkably noisy, and the vertical component lost half of its gain in 2006.

The sensor problems identified here should have been identified early on, and corrected. We speculate that the problem went unnoticed or undiagnosed because no routine calibrations have been performed at GSN stations. The lack of systematic calibrations, and inspection of calibration results, makes it difficult to identify instrument problems. In addition, the lack of calibrations makes it nearly impossible to repair errors in instrument parameters once a problem has been identified. The symptoms of the STS-1 malfunction on the N–S component were reported earlier (Ekström et al., 2006) and are similar to those observed at other stations; interpretation is complicated by the presence of multiple sensor problems.

Modern seismological analyses require well-calibrated instruments. Amplitude variations of 10% and smaller are interpreted as signals in modern studies that seek to map the attenuating properties of the Earth's interior (e.g., Dalton and Ekström, 2006). Phase anomalies of a few seconds at long periods are similarly interpreted in terms of Earth's elastic structure by numerous authors. Data from SSE have been used in such studies with the assumption that the station is meeting GSN design goals (IRIS, 1985; Lay et al., 2002) with respect to instrument calibration and stability. Clearly it does not, and its failure to do so should be documented. This is particularly important when, as for SSE, the data may at times appear visually to be correct, but actually are faulty.

It is urgent to restore SSE to a state where it generates GSN-quality data. It is especially unfortunate that the STS-2 has not provided quality replacement data, in particular since 2006. It would be fruitful to determine the cause of the sudden loss of gain for the vertical STS-2 component. It is possible that a simple repair or STS-2 sensor replacement would restore baseline broadband functionality at the station. The problems with the STS-1 should be investigated and addressed.

4 References

Dziewonski, A. M., T.-A. Chou, and J. H. Woodhouse, Determination of earthquake source parameters from waveform data for studies of global and regional seismicity, *J. Geophys. Res.*, 86, 2825–2853, 1981.

Ekström, G., A. M. Dziewonski, N. N. Maternovskaya, and M. Nettles, Global seismicity of 2003: Centroid-moment tensor solutions for 1087 earthquakes, *Phys. Earth Planet. Inter.*, 148, 327–351, 2005.

Ekström, G., C. A. Dalton, and M. Nettles, Observations of time-dependent errors in long-period gain at global seismic stations, *Seism. Res. Lett.*, 77, 12–22, 2006.

Ekström, G., and R. W. Busby, Measurements of seismometer orientation at USArray Transportable and Backbone stations, *Seism. Res. Lett.*, 79, 554-561, 2008.

Ekström, G., and M. Nettles, Performance of the GSN station KIP-IU, 1988–2009, Waveform Quality Center Report 2010:2, 2010.

Ekström, G., and M. Nettles, Performance of the GSN station DAV-IU, 1994–2009, Waveform Quality Center Report 2010:7, 2010.

IRIS, *The design goals for a new global seismographic network*, IRIS GSN committee report, 31 pages, 1985.

Lay, T., J. Berger, R. Buland, R. Butler, G. Ekström, B. Hutt, B. Romanowicz, *Global seismic network design goals update 2002*, IRIS GSN committee report, 2002.

Peterson, J., Observations and modeling of background seismic noise, *U. S. Geol. Surv. Open-file Rep. 93-322*, 1–45, 1993.

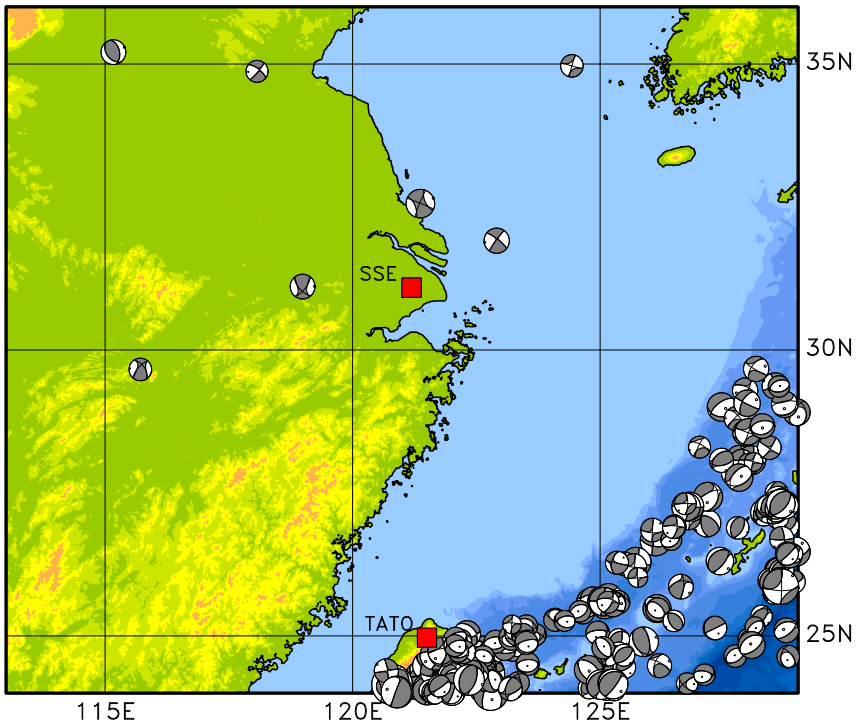

Figure 1: Map showing the location of SSE (red square) near the city of Shanghai in eastern China. Grey focal mechanisms show the locations and moment tensors of earthquakes in the Global CMT catalog. The closest GSN station is TATO-IU, located $\sim$700 km to the southwest in Taipei, Taiwan.

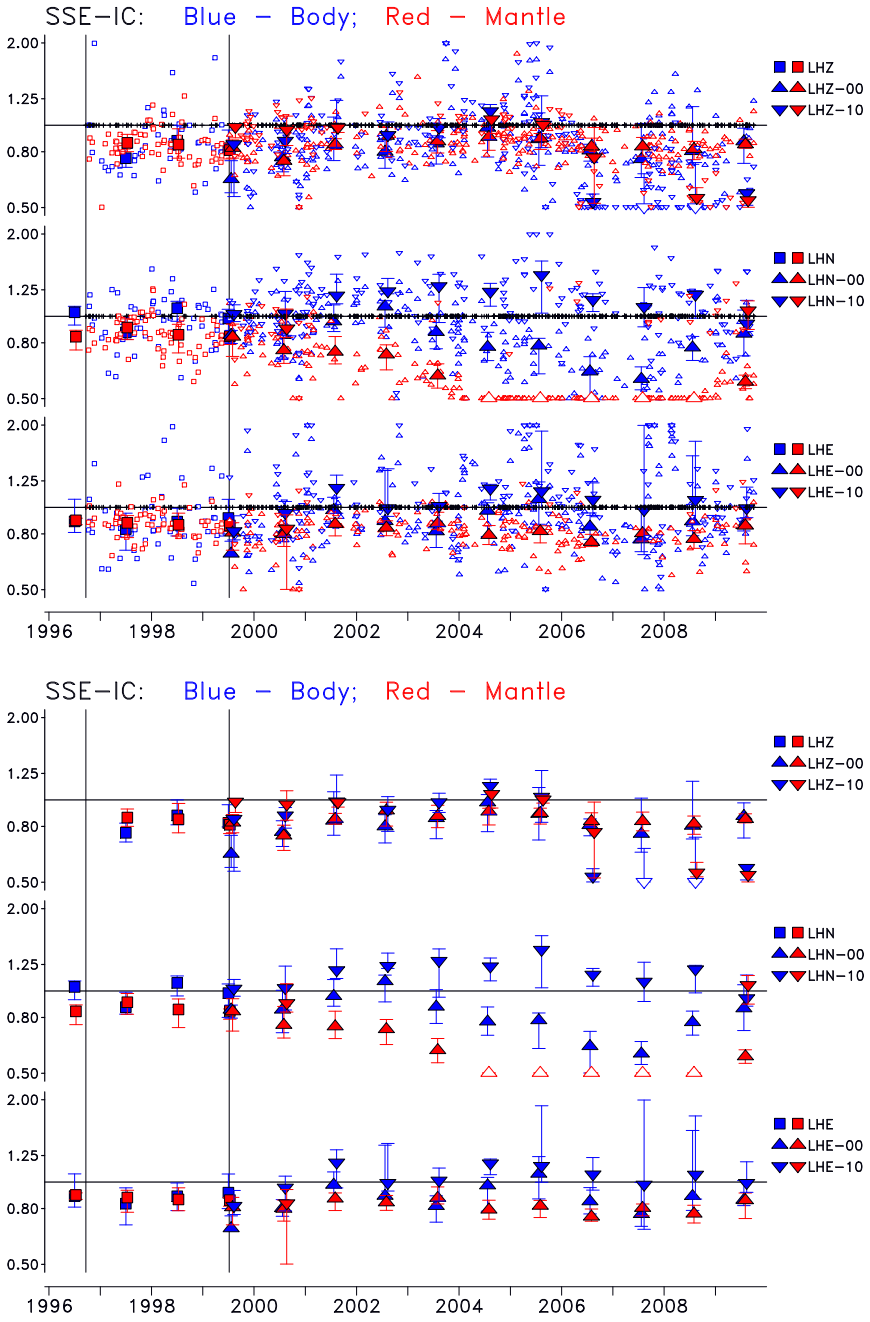

Figure 2: Scaling factors for the various data channels at SSE. Small symbols in top panel show scaling factors for individual traces. Tick marks on the horizontal axes show times of observations for which the correlation was less than 0.75. Large symbols show the median scaling factor for each year, with the error bars corresponding to the range of the second and third quartiles of the scaling factors. The legend on the right identifies the symbol type with a specific channel. A gradual decrease in the long-period scaling factor is seen for the STS-1 N–S component, starting in 2000. A sudden drop of the scaling factor for the vertical component of the STS-2 is seen in 2006. Thin vertical lines show the response epoch boundaries present in the metadata. Bottom panel: same, but showing only the annual median values.

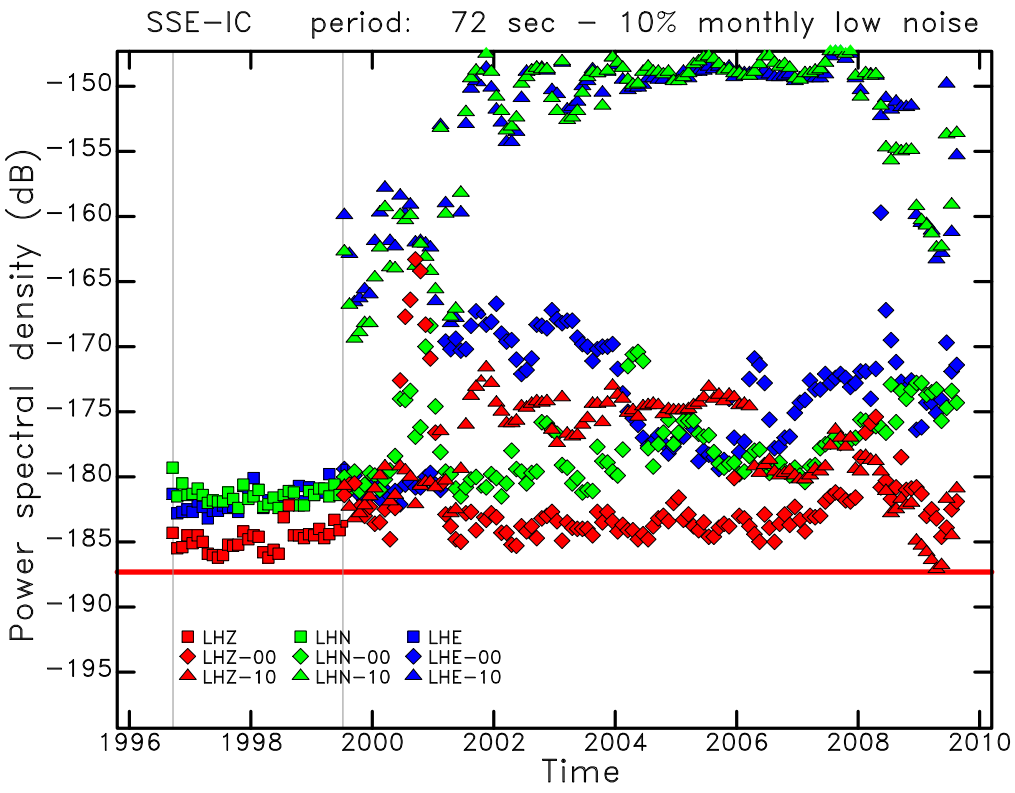

Figure 3: Monthly PSD of ground acceleration at 72-s period for all long-period (LH) channels at SSE for the period 1996–2009. Smaller symbols are used for months with fewer available hourly measurements. Each component and sensor is represented by a distinct symbol and color. The red horizontal line indicates the level of Peterson's (1993) Low Noise Model (LNM) at 72 s. The thin vertical lines show the times of epoch boundaries in the station metadata.

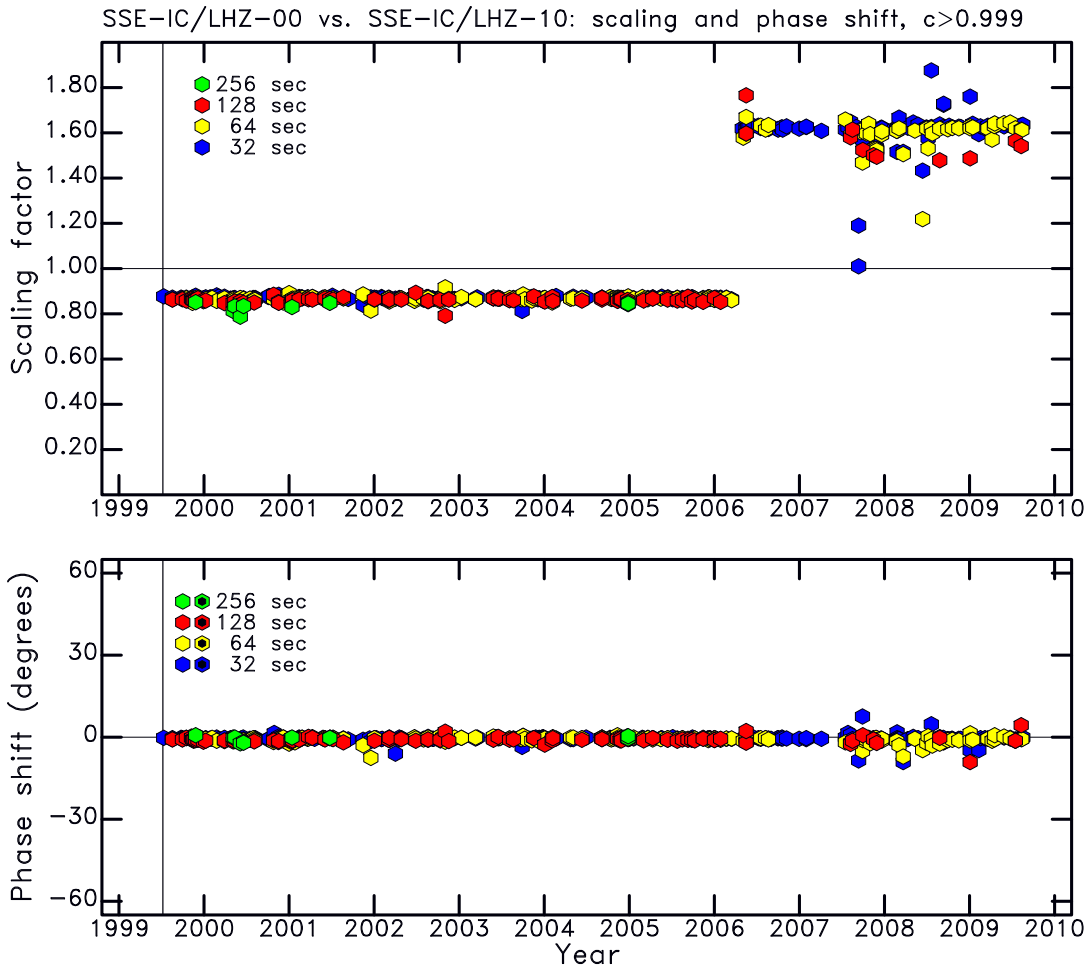

Figure 4: Diagram shows the result of coherence analysis for the vertical components of the STS-1 and STS-2 sensors. Each symbol represents a measurement of coherence for a $M_W \geq 6.5$ earthquake. The minimum coherence plotted is indicated by c. The scaling and phase shift between the two time series is shown at four different periods. The consistent deviations of the coherence measurements from a scaling factor of 1.0 during 1999–2006 suggests an error in the gain of the STS-1. In 2006, the STS-2 vertical component appears to have lost half its gain. The thin vertical lines show the times of epoch boundaries in the station metadata.

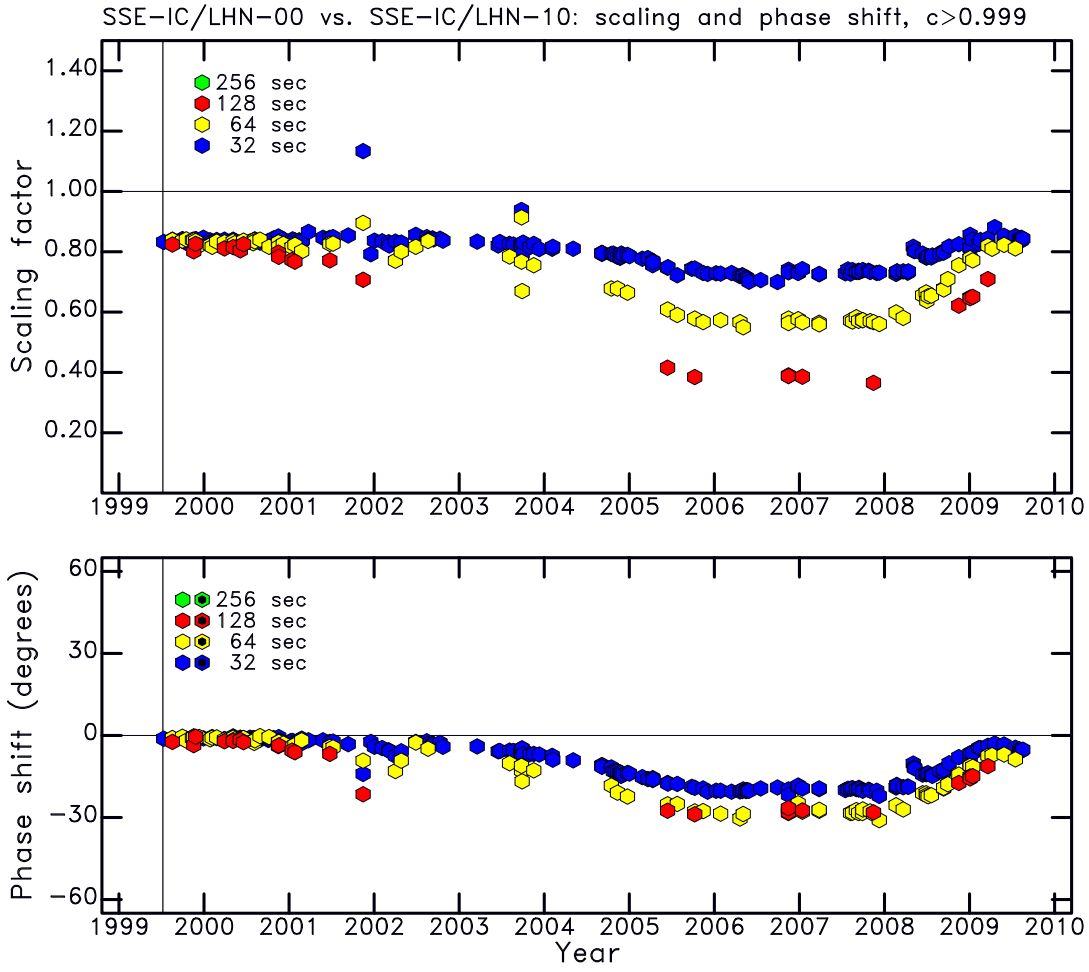

Figure 5: Same as Figure 4, but for the North-South components. Large and time-variable response errors are evident, reflecting a time-dependent loss of long-period gain of the STS-1. The phase response is also affected.

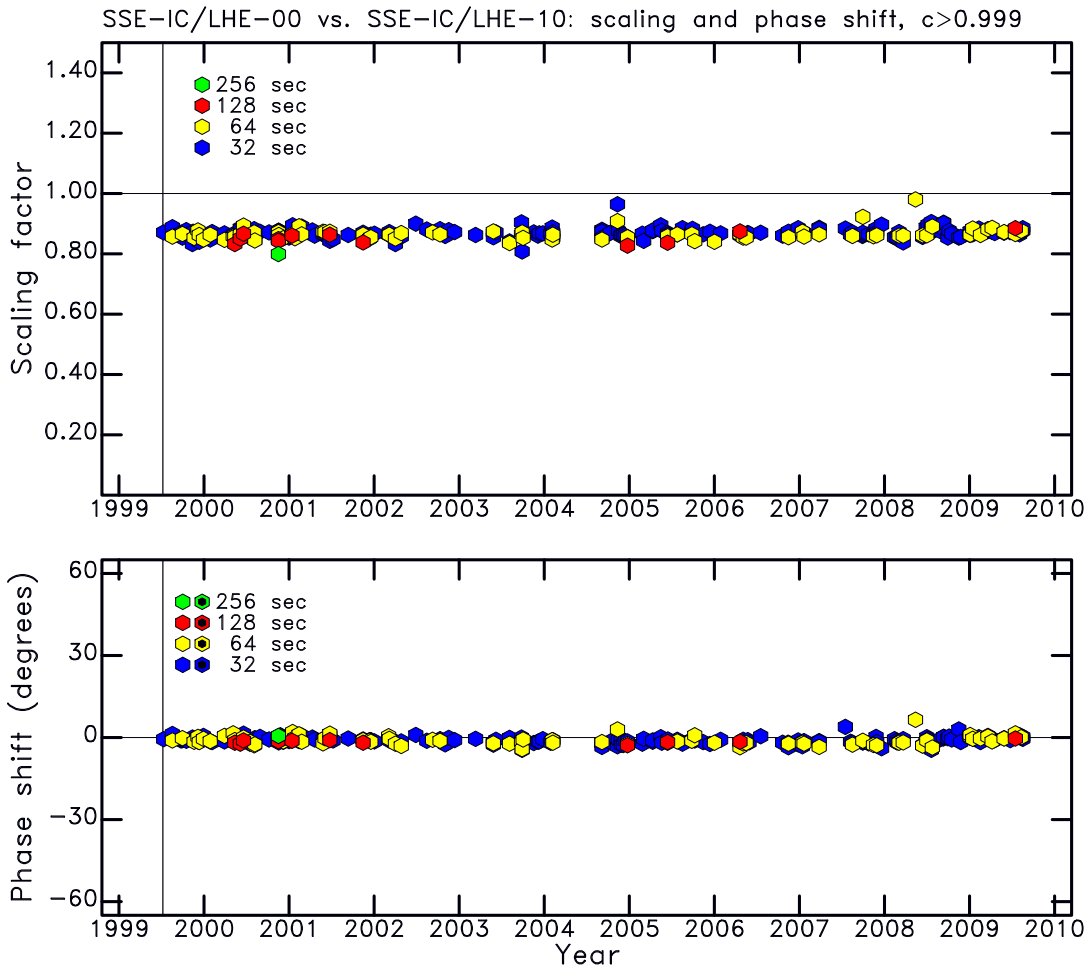

Figure 6: Same as Figure 4, but for the East-West components. The observations are consistent with an error of about 15% in the gain of the STS-1.

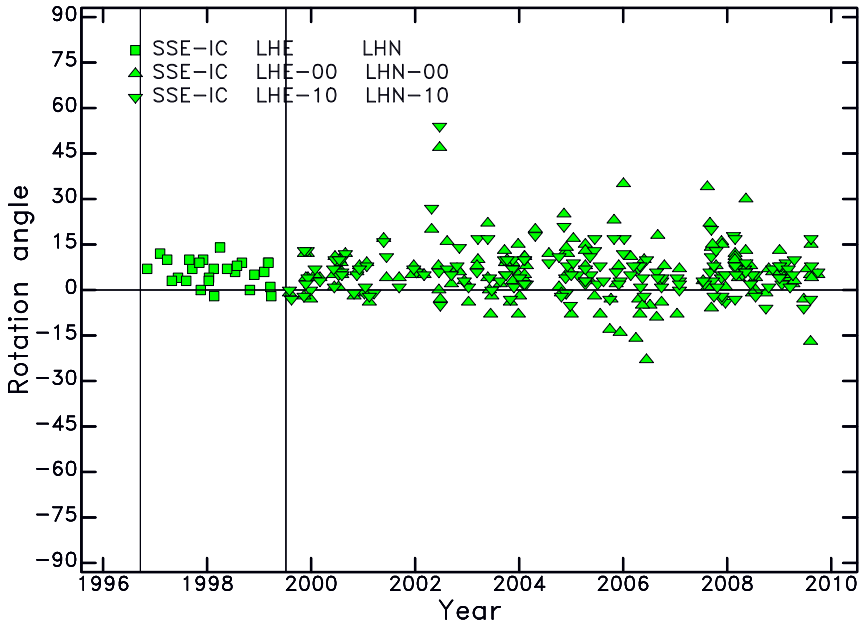

Figure 7: Individual measurements of polarization angle as a function of time. All measurements for the period of operation are shown. Symbols represent measurements obtained in the surface-wave band of the CMT analysis. More than 50% of the observations lie in the range $+1^\circ$ to $+11^\circ$ for the STS-1 sensor and in the range $+2^\circ$ to $+10^\circ$ for the STS-2 sensor, suggesting that both sensors are misoriented by $\sim 5^\circ$. The thin vertical lines show the times of epoch boundaries in the station metadata.

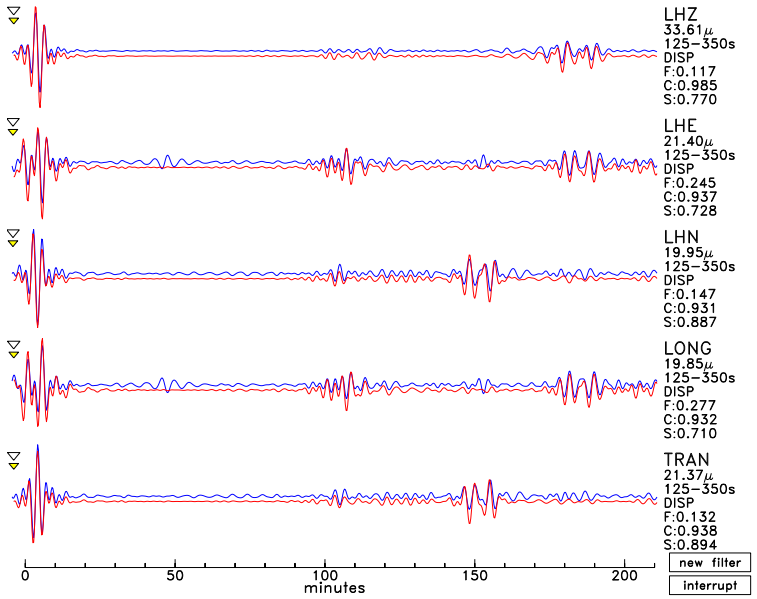

Figure 8: Observed and synthetic mantle-wave seismograms for an earthquake on December 2, 1996. The fit is very good, and noise levels are low on all three components. The scaling factors indicate a problem with the absolute gain of the STS-1 sensor.

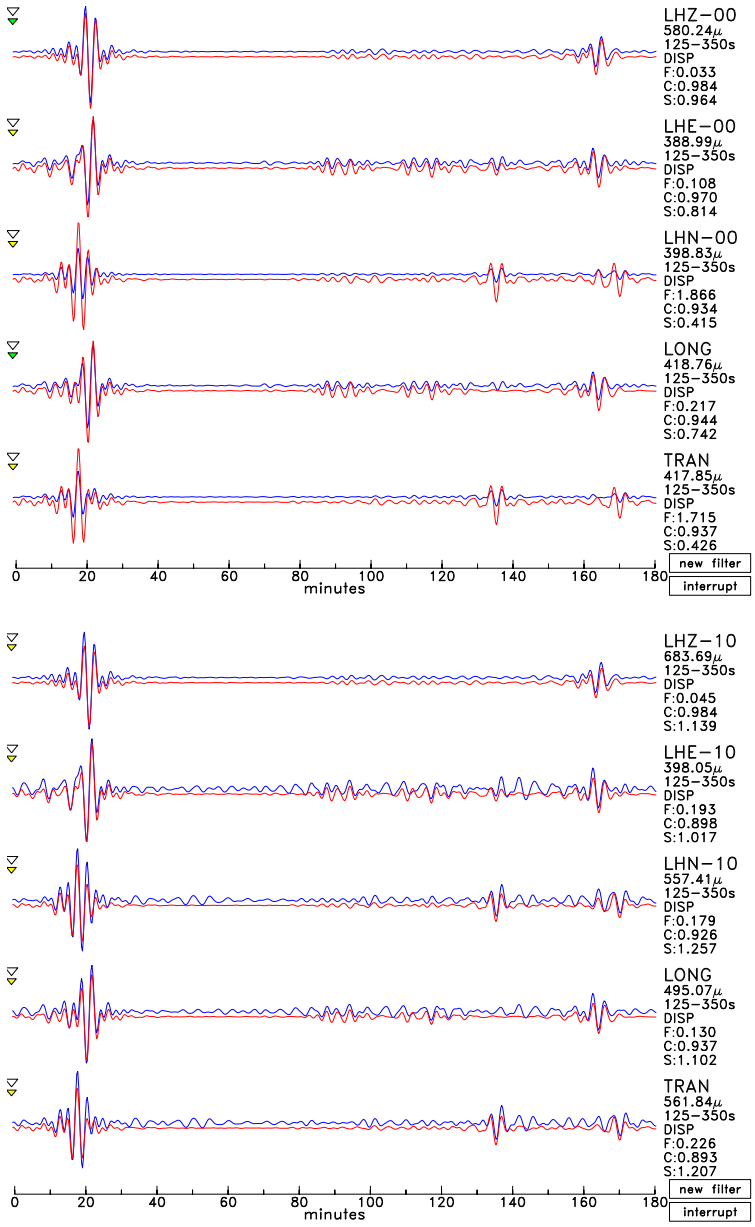

Figure 9: (Top) Observed (STS-1) and synthetic mantle-wave seismograms for an earthquake on October 8, 2005. The correlation between observed and synthetic signals (C in right-hand column) is high, but the scaling factors deviate significantly from 1.0, especially for the N–S component, which shows a loss of long-period gain. (Bottom) Observed (STS-2) and synthetic mantle-wave seismograms for the same earthquake, but recorded on the STS-2 seismometer. The fit to all three components is good, although noise levels are high.

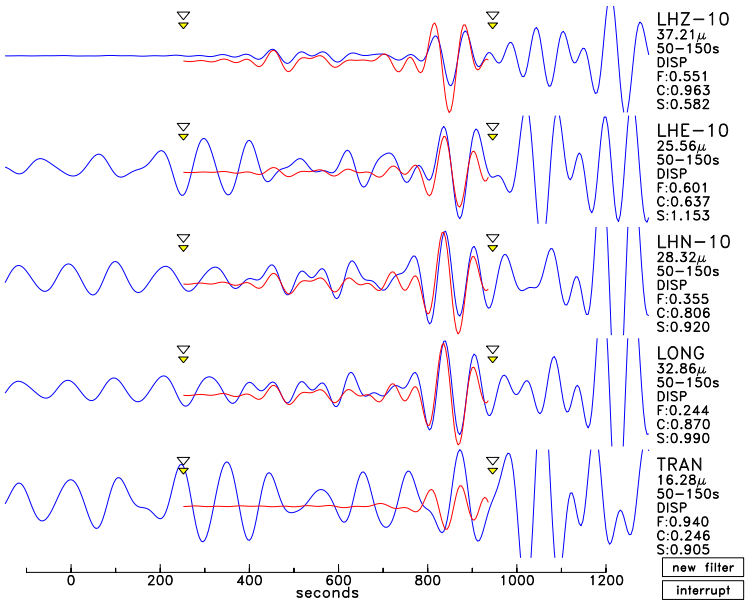

Figure 10: Observed and synthetic body-wave seismograms for an $M_W = 7.0$ earthquake on September 2, 2009 for the STS-2 sensor. The scaling factor for the vertical component is small, reflecting the factor-of-two loss of gain for this component. The noise levels on the horizontal components are very high.